THE JOURNAL OF PHYSICAL CHEMISTRY B

Article

pubs.acs.org/JPCB

Melting of Hydrogen Bonds in Uracil Derivatives Probed by Infrared Spectroscopy and ab Initio Molecular Dynamics

Zsolt Szekrényes,*[,†] Katalin Kamarás,[†] György Tarczay,[‡] Anna Llanes-Pallás,[§] Tomas Marangoni,[§] Maurizio Prato,[§] Davide Bonifazi,[§,∥] Jonas Björk,[⊥,#] Felix Hanke,[⊥] and Mats Persson[⊥,¶]

[†]Institute for Solid State Physics and Optics, Wigner Research Centre for Physics, Hungarian Academy of Sciences, H-1525 Budapest, Hungary

[‡]Laboratory of Molecular Spectroscopy, Institute of Chemistry, Eötvös Loránd University, H-1518 Budapest, Hungary

[§]Dipartimento di Scienze Farmaceutiche and INSTM UdR di Trieste, Università degli Studi di Trieste, Piazzale Europa 1, 34127 Trieste, Italy

[∥]Department of Chemistry, University of Namur (FUNDP), Rue de Bruxelles 61, 5000 Namur, Belgium

[⊥]The Surface Science Research Centre, The University of Liverpool, Liverpool L69 3BX, U.K.

[#]Department of Physics, Chemistry, and Biology, IFM, Linköping University, 58183 Linköping, Sweden

[¶]Department of Applied Physics, Chalmers University of Technology, 41296 Göteborg, Sweden

Supporting Information

ABSTRACT: The thermal response of hydrogen bonds is a crucial aspect in the self-assembly of molecular nanostructures. To gain a detailed understanding of their response, we investigated infrared spectra of monomers and hydrogen-bonded dimers of two uracil-derivative molecules, supported by density functional theory calculations. Matrix isolation spectra of monomers, temperature dependence in the solid state, and ab initio molecular dynamics calculations give a comprehensive picture about the dimer structure and dynamics of such systems as well as a proper assignment of hydrogen-bond affected bands. The evolution of the hydrogen bond melting is followed by calculating the C═O···H−N distance distributions at different temperatures. The result of this calculation yields excellent agreement with the H-bond melting temperature observed by experiment.

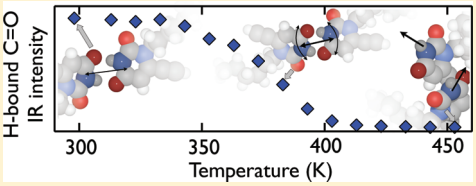

INTRODUCTION

The formation and breaking of hydrogen bonds is one of the most fundamental processes in biology, chemistry, and materials science. For example, H-bonding is responsible for the formation of the DNA double helix and for the highly unusual phase diagram of water or the secondary and tertiary structures in proteins; it is therefore at the very heart of life sciences. Furthermore, with the continuous down-scaling of technology in mind, the self-assembly and molecular recognition properties of H-bonds have found their way into the fabrication of nanoscale materials and devices.[1] It is therefore imperative to understand the microscopic mechanisms that lead to the formation and dissolution of H-bonds, in particular their temperature dependence. These processes are primarily driven by thermal fluctuations, which are particularly large in H-bonded systems as they include very light atoms and a relatively shallow and anharmonic potential energy well.

To study this process in a simple and controlled manner, numerous different systems have been suggested, for example, short polypeptide segments[2,3] or custom-designed molecular modules.[4−7] In this context, it is crucial to have detailed information from both experiment and theory so that the observed thermal fluctuation effects can be properly assigned. Systems that are particularly suited for the controlled study of hydrogen bond formation are small cyclically bonded nucleic acid base pairs, which play an important role as basic building blocks in both biology and nanotechnology.[1] Because of the many functional groups of such purines and pyrimidines taking part in hydrogen bonds, there are many ways that both homomolecular[8] and heteromolecular pairing can be exploited in, for instance, defect-free 2D supramolecular network formation with long-range order.[9−11]

In this study, we investigate the stability and dissociation dynamics of hydrogen bonds by studying a pair of uracil-derivative molecular modules. Uracil-based molecular building blocks have already shown their potential as basic components in supramolecular chemistry,[5,9,12−16] which means that their stability and breakdown mechanisms are of technological importance. In this context, infrared (IR) spectroscopy is very effective in the study of such hydrogen bonded complexes.[17,18] Special methods like matrix isolation (MI) spectroscopy combined with a more conventional IR spectroscopic method provide unique characterization opportunities as they permit the study of the molecular units both in their aggregated and

Received: December 15, 2011
Revised: March 15, 2012
Published: March 21, 2012

free state. MI-IR spectroscopy in particular is a powerful method to measure an almost perturbation-free spectrum of isolated molecules.[19] Choosing appropriate conditions, these spectra can be free from signs of aggregated species even in the case of strong intermolecular interactions.[20,21]

Two uracil-type molecules (Scheme 1) were chosen for our combined experimental and theoretical IR spectroscopy investigation: 1-hexyl-6-ethynyluracil (1H6EU) and 1-hexyl-6-iodouracil (1H6IU). The two molecules contain identical hydrogen bond-forming functional groups but differ in the functional group attached to atom 6 of the central aromatic ring (see Scheme 1). MI-IR characterization was performed on isolated molecules and compared to spectra in the solid state, where aggregation is present.[22,23] On heating the solids, we observe a sudden drop in intensity of certain spectral lines with temperature, which we attribute to the melting or disruption of H-bonds. The combination of IR studies with temperature-controlled ab initio molecular dynamics simulations, e.g., in the canonical (*NVT*) ensemble, allows the unambiguous but nontrivial assignment of the temperature-dependent spectral peaks.

Scheme 1. 1-Hexyl-6-ethynyluracil (1H6EU) (left) and 1-Hexyl-6-iodouracil (1H6IU) (right) Have Identical Functional Groups Forming Hydrogen Bonds (Carbonyl and Amine Groups)[a]

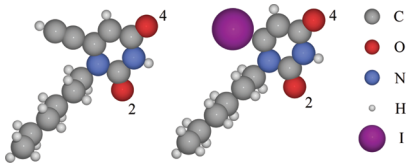

[a]The molecules are shown in the diketo form. We indicate the two carbonyl groups including carbon atoms 2 and 4, respectively, which may participate in different hydrogen bonding motifs.

MATERIALS AND METHODS

Materials and Experimental Methods. 1H6EU and 1H6IU were prepared according to previously published procedures[9,12,14] (see Supporting Information for details). Temperature-dependent infrared spectra in the solid state were recorded in powders ground in KBr pellets. Mixing with KBr dilutes the material so it becomes transparent to IR light, but the grain size in the pellets (~1 μm) ensures that they still can be regarded as solids, preserving the structure. Therefore, in the rest of the article, we will refer to these samples as solids.

The matrix isolation (MI) setup is described in detail elsewhere.[24,25] Briefly, the evaporated sample was mixed with argon (Messer, 99.9997%) before deposition onto an 8−10 K CsI window. The gas flow was kept at 0.07 mmol min^{-1}, while the evaporation temperature was optimized to get the shortest possible deposition time and keep the concentration low enough to minimize the formation of dimers during deposition. The optimum temperature was 353 ± 5 K for 1H6EU and 393 ± 5 K for 1H6IU. Under these circumstances, the sample consists predominantly of isolated molecules, with only a small amount of aggregated species present. Therefore, comparing MI-IR spectra with solid-state KBr pellet spectra allows us to study the effect of aggregation. Three different FTIR instruments were used (Bruker Tensor 37 and IFS66v for the temperature dependence with 2 cm^{-1} resolution and MCT detector, Bruker IFS 55 for MI with 1 cm^{-1} resolution and DTGS detector.) All spectra were taken in the 400−4000 cm^{-1} range with a Ge/KBr beamsplitter. The baseline was corrected by an adjusted polynomial function, the low-intensity atmospheric water vapor lines were removed by subtraction of a water vapor spectrum.

Theoretical Methods. The temperature dependence of the observed infrared spectra and the disruption of the H bonds have been investigated theoretically using ab initio molecular dynamics calculations (AIMD) based on density functional theory, which gives accurate forces and dipole moments. The assignment of the observed modes was based on the vibrational dynamics as provided by AIMD calculations at very low temperatures of about 5 K. At this temperature, the thermal fluctuations are so small that only the harmonic part of the potential energy surface is probed. However, anharmonic effects will be large for high frequency modes involving H atoms for which zero-point motion is so large that anharmonic parts of the potential energy surface are important. For these modes, the harmonic approximation tends to overestimate the vibrational frequencies.

A proper description of any anharmonic effects is only possible by classical AIMD calculations for vibrational modes when thermal fluctuations dominate over the zero point fluctuations corresponding to vibrational energies being less than the thermal energy. In the temperature range of interest for this study this condition strictly corresponds to vibrational frequencies less than 3000 cm^{-1}. The justification for our study of the temperature dependence of the H-bond affected C═O stretch vibration with a frequency of about 1700 cm^{-1} is based on the strong C═O chemical bond, which makes the anharmonic effects small for the lowest lying vibrational states. So, we are here primarily studying the effect of the disruption of the H bonds on the harmonic part of the C═O stretch potential, a frequency region in which the AIMD approach taken here is known to work well.[2]

To find the structures and relative stability of different H-bonding motifs, density functional calculations were performed with the all-electron numeric local orbital package FHI-aims,[26] using the tier1 basis sets (equivalent to double-numeric plus polarization, with *spspd* basis functions for elements C, N, and O, and *ssp* for H) available with that package. The light integration settings of FHI-aims have been used, e.g., the electronic density has been expanded in atom-centered spherical Lebedev grids containing up to 302 points per grid.[26] These settings generally provide a very good description of the molecular geometry and energy differences but at a small fraction of the cost of a fully converged calculation. All possible hydrogen-bonded motifs for the dimers of 1H6EU were optimized to within 0.01 eV/Å using the PBE exchange correlation functional[27] with the Tkatchenko−Scheffler dispersion correction to account for van der Waals interactions.[28] The noncovalent bonding motifs in the computed structures are very similar to those in the S22 fit set,[29] which is used to parametrize the damping function of the dispersion correction. Therefore, we expect that dispersion correction performs very well for our particular systems.[30]

Ab initio molecular dynamics (AIMD) calculations were performed for all three dimer structures of 1H6EU and 1H6IU at different temperatures to obtain vibrational spectra. For the lowest energy dimer structure, additional simulations at 5 K, 383 K, and 453 K were used to calculate the temperature dependence of its spectrum. All AIMD calculations use the

dx.doi.org/10.1021/jp212115h | J. Phys. Chem. B 2012, 116, 4626−4633

Scheme 2. Three Investigated Dimer Configurations of 1H6EU in the AIMD Study (The Same Structures Were Considered Also for 1H6IU)

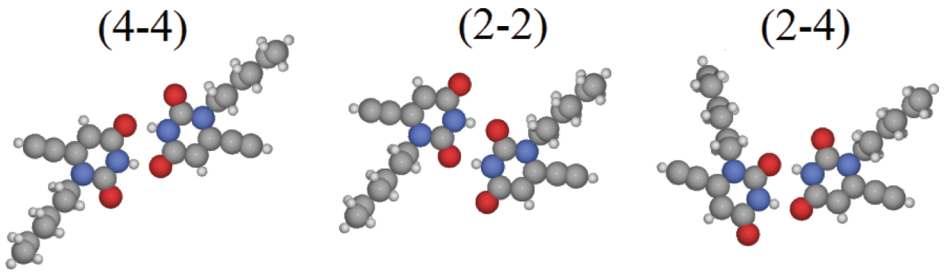

Bussi–Donadio–Parrinello thermostat (BDP)[31] with a relaxation time of 150 fs and a time-step of 1 fs. Unlike other commonly used thermostats in molecular dynamics simulations, the BDP implementation has been shown to preserve the autocorrelation functions required for the vibration analysis,[31] while also allowing to keep the temperature fluctuations reasonably small. The calculations were run for 22 ps, where the first 2 ps were used to thermalize the system and the remaining 20 ps for sampling. An additional simulation for the most stable dimer up to 30 ps showed that 20 ps is sufficient to converge the spectrum. Scheme 2 presents the three dimer conformations considered in the calculation. The N–H (3) and one C═O (2 or 4) group are always involved in hydrogen bond formation, while the other C═O group is free. We use the notation of Biemann, Häber, and Kleinermanns[32] for the carbonyl groups as well as the dimers: in the latter case, we indicate the labels of the carbon atoms of the carbonyl groups taking part in the hydrogen bond. The situation in these two compounds is simplified compared to that of uracil[22,23] because the N_1 atom is blocked by the side chains and cannot take part in hydrogen bonds; thus, the general bonding motif is that connecting two C═O groups with one N–H group each.

The infrared intensity of the vibrational spectra was calculated from the Fourier transform of the dipole–dipole autocorrelation function via the following relationship:[2,33]

$$I(\omega) \approx \omega^2 \int dt e^{i\omega t} \langle \mathbf{d}(t)\mathbf{d}(0)\rangle \quad (1)$$

where $\mathbf{d}(t)$ is the molecular dipole moment at time t. The spectrum $I(\omega)$ has then been broadened with a Gaussian function by 5 cm^{-1}. The ω^2 term arises from correcting the quantum mechanical absorption strength by a harmonic quantum correction factor to the classical line-shape function.[34,33]

The characterization of vibrational peaks in the calculated dipole spectra is a nontrivial task. Here, it was done by identifying a set of representative bond coordinates, e.g., bond distances or bond angles, and extracting their time dependence $A(t)$ from our AIMD trajectories using the Atomic Simulation Environment.[35] The character of a given mode in terms of various bond coordinates is given by the relative spectral strengths of the vibrational peak in the Fourier transforms $A(\omega)$ of these coordinates, as demonstrated in Figure 1 (see also Supporting Information for additional assignments). Figure 1 also shows the corresponding harmonic spectrum. For our 5 K MD simulations, the molecules only sample the harmonic region of the potential energy surface. This is reflected in the good correspondence between the harmonic and molecular dynamics vibration spectra, which agree to within 10 cm^{-1}. Moreover, our approach toward identifying vibrational modes

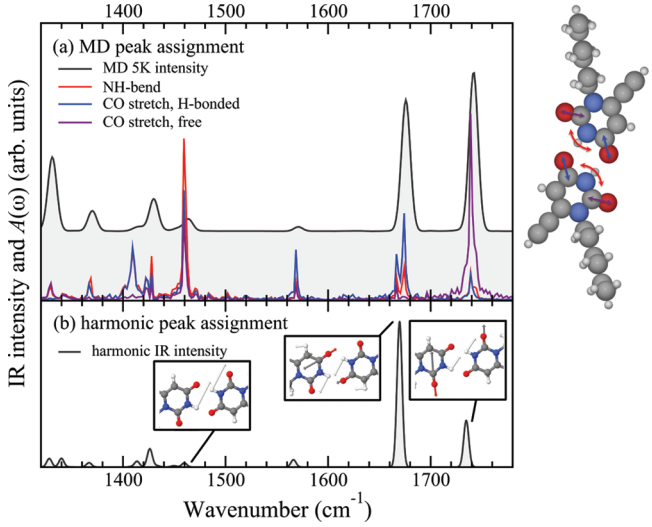

Figure 1. (a) Illustration of the procedure used to assign the peaks in molecular dynamics spectra: each colored line shows the Fourier transform of a given collective coordinate of the (4–4) dimer simulated at 5 K; see molecular model on the right. The shaded area shows the full infrared intensity computed from the MD simulation and offset by a constant for comparison. (b) Corresponding IR intensity calculated within the harmonic approximation using finite differences. The peaks assigned to eigenmodes with the most prominent C═O stretch and/or N–H bend character are indicated, with the atomic motions illustrated with arrows in the molecular models for each of these three modes.

can also be used for a given vibrational mode to identify the coupling between the collective coordinates, e.g., between the N–H bend and the two C═O stretches at 1460 cm^{-1} for 1H6EU where the spectrum of all three bond coordinates has peaks in Figure 1. This is also reflected in the normal-mode analysis, where the N–H bend also has a small component of the C═O stretch modes and vice versa.

RESULTS AND DISCUSSION

Matrix Isolation Results. Figures 2 and 3 present the experimental IR spectra of 1H6EU and 1H6IU, respectively, in the solid state (black curve, recorded at 298 K) and matrix isolation infrared (MI-IR) spectra of isolated monomers (red curve, recorded in argon matrix at 8 K). Mode assignment of the MI-IR spectra was done by comparing these to the theoretical spectra calculated for monomers at 5 K, while the assignments of solid state spectra were obtained by comparison with the theoretical spectra calculated for different dimer configurations. In the solid phase at 298 K, the sample state can be considered a static assembly of dimers with H-bonds being

dx.doi.org/10.1021/jp212115h | J. Phys. Chem. B 2012, 116, 4626–4633

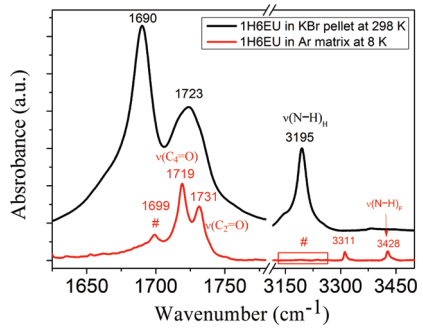

Figure 2. Direct observation of the effect of H-bonds on 1H6EU: comparison between the solid state spectrum (at room temperature, black) and monomers (in Ar matrix, red). Peaks marked with # are from the very low amount of dimers formed during Ar matrix formation. All the spectra were baseline corrected and shifted vertically for clarity. Subscripts 2 and 4 refer to the corresponding carbonyl groups according to Scheme 1, while subscripts F and H denote the free and hydrogen bonded nature of the vibrations, respectively.

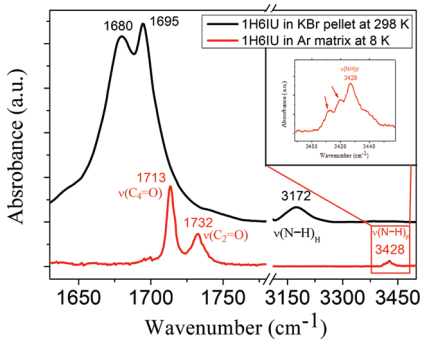

Figure 3. Solid state spectrum at 298 K (black curve) and matrix isolation spectrum at 8 K (red curve) of 1H6IU. Subscripts 2 and 4 refer to the corresponding carbonyl groups according to Scheme 1, while subscripts F and H denote the free and hydrogen bonded nature of the vibrations, respectively.

the main intermolecular interaction,[22,23] which affects the corresponding IR bands. Lowering the temperature causes line narrowing in the solid state but does not affect the positions considerably. Therefore, a direct comparison between the solid state and MI-IR spectra is possible even if the temperature is different.

In the experimental MI-IR spectrum of 1H6EU, the bands at 1719 and at 1731 cm^{-1} belong to the free C_4=O and C_2=O (according to Scheme 1) vibrations of the monomer, respectively. The comparison of experimental and theoretical band assignments is presented in Table 1.

One of the bands in the matrix isolation spectrum of 1H6EU in Figure 2 (marked with #, at 1699 cm^{-1}) merits a more detailed analysis. We have considered two possibilities for the assignment of this band; either the presence of another tautomer or a small number of dimers. Although the temperature dependence in the solid phase (detailed in the next subsection) did not reveal the presence of other tautomers either for 1H6EU or for 1H6IU, tautomerization can occur during sublimation or in the gas phase.[36] Our calculations show that the total energies of the enol tautomers relative to that of the diketo tautomer are high (above 50 kJ mol^{-1}, see Supporting Information, Figure S11), which is in agreement with previous experimental and theoretical results for other uracil derivatives.[36−42] These studies show that the diketo form of uracil is the most stable and predominant tautomer in the gas phase, in solution and in the solid state; hence, we exclude the presence of other tautomers in the matrix. Instead, we conclude that the band at 1699 cm^{-1} can be assigned to the C=O mode of the hydrogen-bonded isolated dimers, which are present in the matrix in a small amount.

Figure 3 presents the solid state spectrum (black curve) and the matrix isolation spectrum (red curve) of 1H6IU. As for 1H6EU, the band assignment of the MI-IR spectrum was performed by comparing with the theoretical spectrum of the monomer of this molecular module. We assign the band located at 1713 cm^{-1} to a C_4=O stretch and the one at 1732 cm^{-1} to a C_2=O stretch. Comparison of matrix isolation spectra of 1H6EU and 1H6IU is presented in Table 2. While the C_2=O bands are at the same position in both cases, the C_4=O bands show a 6 cm^{-1} difference between the two molecules,which is caused by the different masses of the ethynyl group and iodine atoms attached to C_6.

To obtain detailed information about the dimer structures of 1H6EU and 1H6IU, we considered three different dimer structures in the theoretical calculations for each of the molecular modules, illustrated for 1H6EU in Scheme 2. Table 3 presents the calculated binding energies for the different configurations, which shows that the (4−4) dimer structure is energetically most stable for both 1H6EU and 1H6IU. This structure is identical to that in crystalline uracil.[22,23] Furthermore, the relative energy hierarchy between the different dimers remains the same for 1H6EU and 1H6IU. Thus, the different functional groups on atom 6 (according to Scheme 1) do not have a significant effect on the hydrogen bonds. This result is also in agreement with results derived

Table 1. Mode Assignments for the Peaks in the MI-IR Spectrum of Isolated 1H6EU[a]

$\tilde{\nu}_{EXP}$ (cm^{-1})	$\tilde{\nu}_{AIMD}$ (cm^{-1})	assignment
3428	3587	ν (N−H)
3311	3478	ν (C−H)
1731	1742	ν (C_2=O)
1719	1718	ν (C_4=O)

[a]Experimental values were derived from the spectrum recorded at 8 K, while theoretical values were calculated by MD simulation at 5 K.

Table 2. Vibrational Frequency and Mode Assignment of Matrix Isolation Spectra of 1H6EU and 1H6IU Monomers

sample	ν(C_4=O) (cm^{-1})	ν(C_2=O) (cm^{-1})	ν(N−H) (cm^{-1})
1H6EU	1719	1731	3428
1H6IU	1713	1732	3428

Table 3. Formation Energies of the Different Isolated Dimers for 1H6EU and 1H6IU, Calculated As the Difference between the Energy of a Structurally Optimized Dimer and Two Structurally Optimized Monomers

dimer	1H6EU (kJ mol^{-1})	1H6IU (kJ mol^{-1})
(4−4)	−62	−63
(2−2)	−56	−56
(2−4)	−58	−59

dx.doi.org/10.1021/jp212115h | J. Phys. Chem. B 2012, 116, 4626−4633

from chloroform solution spectra of 1-cyclohexyluracil by Biemann, Häber, and Kleinermanns.[32]

In Table 4 experimental and computed frequencies are shown for the (4−4) structure of 1H6EU. Note that the experimental value for $\nu(C_2{=}O)$ for the dimers is equal to the corresponding mode in the isolated molecule, suggesting that it is not at all affected by the surrounding H-bonds.

Table 4. Mode Assignments of Isolated Dimers in the Experimental (8 K) and Calculated (5 K) IR Spectrum of the Most Stable (4−4) Dimer Structure of 1H6EU[a]

$\tilde{\nu}_{EXP}$ (cm^{-1})	$\tilde{\nu}_{AIMD}$ (cm^{-1})	assignment
1731	1742	$\nu\ (C_2{=}O)_F$
1699	1676	$\nu\ (C_4{=}O)_H$

[a]Subscripts 2 and 4 refer to the corresponding carbonyl groups according to Scheme 1, while subscripts F and H denote the free and hydrogen bonded nature of the vibrations, respectively.

Temperature Dependence. Temperature-dependent infrared spectroscopic investigations using solid samples can be used for the characterization of the stability of hydrogen bonded systems as the behavior of bands shows how the hydrogen bonds become weaker or entirely disrupted at elevated temperature:[9] with increasing temperature, the hydrogen bond affected bands decrease in peak height and shift to higher wavenumbers. This phenomenon is attributed to the stiffening of the potential energy minimum for the H-atom as the hydrogen bond is being broken. Moreover, the electron on the H-atom becomes more localized and more strongly bound, which decreases its polarizability and, consequently, the intensity of the band.

Our study also shows that the coexistence of different dimer conformers at elevated temperatures needs to be taken into account in the analysis of the IR spectra. Here, we focus on the temperature dependence of the modes affected by hydrogen bonding that are well described by our theoretical approach, i.e., only the C═O stretching vibrations. Figure 4 presents the temperature-dependent spectra of 1H6EU from room temperature up to 453 K. Apparently, the spectra contain two components: one hydrogen bonded C═O stretching band at 1690 cm^{-1} and one free C═O band centered at 1723 cm^{-1} (according to Scheme 2, just one C═O is H-bonded in all dimer conformers). Above 353 K, a strong decrease in the peak height can be observed for the hydrogen bonded band (C═O band at 1690 cm^{-1}) along with a slight shift to higher wavenumbers. Above 403 K, the free and hydrogen bonded C═O merge into one single broad band. The inset of Figure 4 shows the peak height of the 1690 cm^{-1} band as a function of temperature. From the inset, it can be seen that the peak height starts to decrease from 353 K with a more pronounced decrease above 383 K.

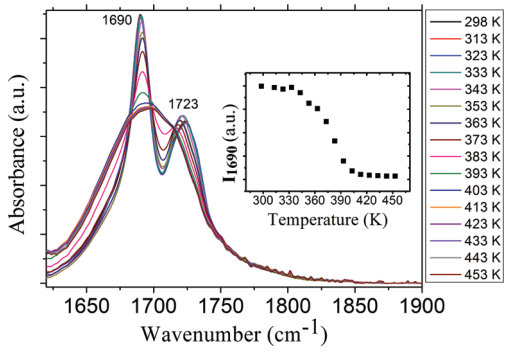

Figure 4. Experimental temperature dependence of the solid state spectrum of 1H6EU. Inset: peak height at 1690 cm^{-1} as a function of temperature.

We observe that the peak height at 1690 cm^{-1} decreases sharply at 353 K (inset in Figure 4) indicating a close correlation between the melting temperature of hydrogen bonds in the solid and the sublimation temperature under MI conditions. As the disruption of the secondary bonds strongly affects the cohesion energy of the solid, it is not surprising that the melting of the hydrogen bonds occurs in the same temperature region as the sublimation in the matrix isolation experiment, i.e., the temperature where the isolated molecules enter the argon stream.

Figure 5 shows the temperature dependence of the solid state spectra of 1H6IU in the C═O stretching region. At room temperature, both free and hydrogen bonded C═O bands are at lower wavenumber than in 1H6EU (Figure 4). There is another difference between the spectra of the two molecules: while the H-bonded C═O band of 1H6EU is more intense than the free one, the H-bonded C═O band of 1H6IU is less intense than the free one. As the temperature is increased, the H-bond affected C═O bands shift to higher wavenumbers, while the free C═O vibration at 1695 cm^{-1} remains unchanged. The inset of Figure 5 shows the intensity of the H-bonded C═O stretch mode at 1680 cm^{-1} as a function of temperature. Similar behavior as for 1H6EU can be observed for 1H6IU in the solid state spectra in the temperature region around the sublimation temperature deduced from the MI-IR experiment (393 ± 5 K for 1H6IU; inset of Figure 5). Drastic changes occur just below 393 K indicating the correlation between sublimation and H-bond melting temperature mentioned above.

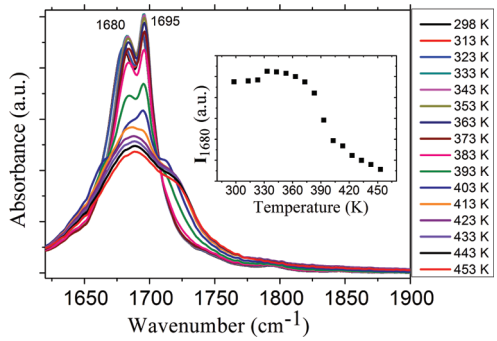

Figure 5. Experimental temperature dependence of the infrared spectrum in the C═O stretching region for solid 1H6IU. Inset: peak height of 1680 cm^{-1} as a function of temperature.

Figure 6 presents the experimental temperature dependence of the solid state spectrum for 1H6IU between 383 and 413 K. In the C═O region, two new bands appear at 1664 and at 1713 cm^{-1}. Such a behavior is not characteristic for either 1H6EU or the energetically most stable dimer (according to Table 2). This is an indication that, before the entire disruption of hydrogen bonds, a coexistence between different dimer conformers can occur in the solid state.

In Figure 7, experimental and theoretical IR spectra for 1H6EU are presented. Panel A represents the experimental results at 298, 383, and 453 K, while panel B shows AIMD

dx.doi.org/10.1021/jp212115h | J. Phys. Chem. B 2012, 116, 4626−4633

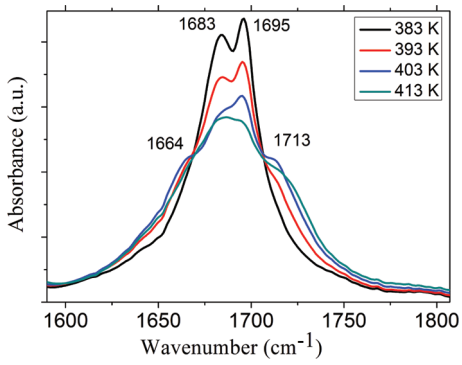

Figure 6. Experimental temperature dependence of the infrared spectrum of the C═O for solid 1H6IU in the range 383−413 K.

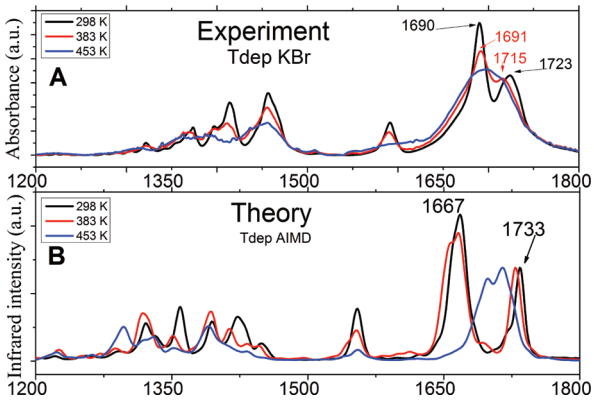

Figure 7. Temperature dependence: (A) measured infrared spectra of solid 1H6EU at 298 K, 383 K, and 453 K; (B) AIMD-computed spectra of the (4−4) dimer.

results for the (4−4) dimer at the same temperatures. In the experimental results, important changes occur with increasing temperature not only in the peak height of the observed H-bonded bands but also in their position. After deconvolution of the experimental spectrum at room temperature, a multicomponent structure of both free and H-bonded C═O stretching bands was revealed (see Supporting Information, Figure S13). The hydrogen bonded C═O band consists of two components, at 1669 and 1689 cm^{-1}. Apparently, the free C═O band contains three components at 1715, 1723, and 1732 cm^{-1}, respectively. Comparing the free C═O peaks to the matrix isolation results of the monomers, it can be seen that the components at 1715 and 1732 cm^{-1} correspond to the free C_4═O and C_2═O vibrations (1719 and 1731 cm^{-1} for the matrix isolation results).

At an elevated temperature of 383 K, the spectrum deconvolution shows an important change in the multicomponent structure (Figure S14 in the Supporting Information). Just four components are found at this temperature (1670, 1691, 1717, and 1731 cm^{-1}), the 1723 cm^{-1} component is completely missing. Such a change with temperature is an indication that the 1723 cm^{-1} band represents a hydrogen bonded component of a different dimer conformer according to Scheme 2 and Table 3. This behavior is an indication that, at given temperatures, different dimer conformers coexist in the solid phase. Moreover, this conclusion is corroborated by the following results from AIMD calculations. To compare the different calculated AIMD infrared spectra (Figure 7B), we normalized their peak height to the free C═O band at 1733 cm^{-1} at room temperature. Similar behavior to the experimental results is observed; above 383 K, the free and H-bonded C═O bands merge into one broader band.

As in the experimental results, a multicomponent structure of the C═O band is present in the simulated spectra, given in Figure 8. The analysis of the simulated spectra shows that the

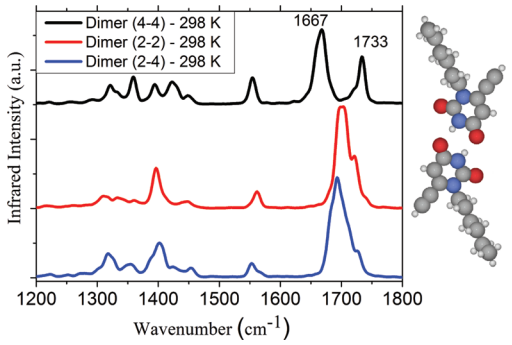

Figure 8. Comparison between simulated IR spectra of the (4−4), (2−2), and (2−4) dimer of 1H6EU at 298 K. The molecular model on the right represents the most stable (4−4) dimer of 1H6EU. The molecular model of the (2−2) and (2−4) dimer is presented in Scheme 2. For an assignment of the different vibrational bands, see the Supporting Information.

number of peaks stems from different symmetric and antisymmetric vibrations arising from the coupling between the two H-bonds present in each dimer (see Supporting Information). For the symmetric (2−2) and (4−4) dimers, one observes two components for the C═O stretch, corresponding to the antisymmetric vibrations of both the free and H-bonded sets of C═O groups. The symmetric vibrations do not yield a significant change in the dipole moment and therefore are not visible in the IR spectra. The same argument shows that the asymmetric (2−4) dimer should have four separate components, which all happen to fall into the same broad peak seen in Figure 8. Interestingly, the strongest red-shift of the asymmetric H-bonded C═O stretch in dimer (4−4) also demonstrates that this dimer is the most favorable conformer at room temperature. However, the number of peaks for each dimer (either two or four) does not correspond to the experimental observation. Our explanation for the apparent disagreement between the number of peaks found in theoretical vibrational spectra for separate dimers on one hand, and the experimental observation on the other, is based on the coexistence of different dimer conformers at room temperature. With increasing temperature, the relative occupancy of different dimer structures is also changing and is much more pronounced in the experimental results.

Figure 9 shows the calculated spectra of the three dimers of 1H6IU at room temperature. The calculated spectrum of the most stable (4−4) structure (black curve) contains four separate components for the C═O stretches, corresponding to two symmetric and two antisymmetric stretches of the four separate C═O bonds. The experimental spectrum in Figure 5, however, shows very broad features that can not be described in terms of the well-separated spectrum of any of the calculated dimers. Therefore, the comparison of experimental temperature spectra of 1H6IU (Figures 5 and 6) with the corresponding calculated spectra of the (4−4) and (2−4) structure (Figure 9 and Supporting Information, Figures S9 and S11) suggests that several different dimer structures are seen in the experiment. A

dx.doi.org/10.1021/jp212115h | J. Phys. Chem. B 2012, 116, 4626−4633

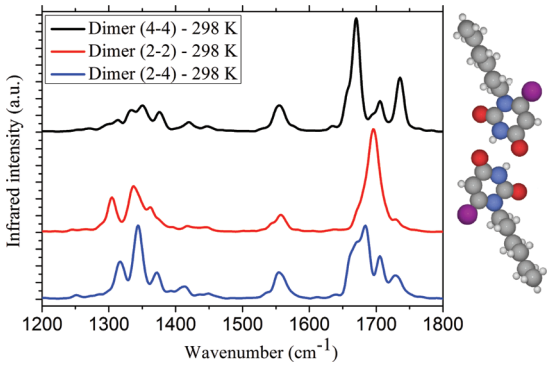

Figure 9. Comparison of the C═O stretching region in the simulated IR spectra of the (4−4), (2−2), and (2−4) dimer of 1H6IU at 298 K. The molecular model on the right represents the most stable (4−4) dimer of 1H6IU.

thermal equilibrium of different bonding motifs should also be expected from the small difference in binding energies.

Further temperature dependent AIMD spectra were calculated for the dimers of both molecules as follows: for 1H6EU, the (4−4) dimer structure at 5 K, 298 K, 383 K, and 453 K as well as for the (2−2) and (2−4) dimer at 5 K, 298 K, and 383 K, while for 1H6IU, the (4−4) dimer structure at 5 K and at 298 K and the (2−2) and (2−4) dimer at 298 K. These theoretical spectra are presented in the peak assignments section of the Supporting Information (Figures S2−S11).

In addition to studying the disruption of the H bonds at elevated temperatures, we are able to give quantitative support for the coexistence of different dimer conformers at room temperature from our AIMD by computing the O···H distances at different temperatures for the different dimer configurations of 1H6EU. The results are shown in Figure 10. First, we consider the temperature dependence of the (4−4) dimer (panel A). At 5 K, the bond lengths are essentially fixed to their minimum energy value of the O···H distance (1.74 Å). At room temperature, the fluctuations of the hydrogen bond lengths are significantly larger, and the highest probability occurs at 1.8 Å. At 383 K, the dimer structure remains stable with a similar bond length distribution as at room temperature, while at 453 K, hydrogen bond disruption occurs. This is evidenced by a broad and uniform bond length distribution which extends to bond lengths well beyond 3 Å. Following the temperature development of the bond lengths for the (2−4) and (2−2) dimers (panels B and C), the double peak structure shows that partial disruption can occur already at room temperature for the (2−4) dimer, while the disruption is nearly complete for the (2−2) dimer. This behavior is even more evident by visualizing the molecular dynamics trajectories, which are available as part of the Supporting Information. The computed difference in thermal stability between different dimer conformers is consistent with the binding energy hierarchy, presented in Table 3. Dimer (4−4) has the largest binding energy and is also the dimer that stays intact at the highest temperatures. For example, at 383 K, dimer (4−4) is intact, although the H-bonds for dimers (2−2) and (2−4) are completely disrupted.

These results support the hypothesis on the coexistence of different dimer conformers at room temperature obtained from the behavior of the experimental spectra. The 1723 cm^{-1} band was assigned to a hydrogen bonded component of a different dimer conformer (Supporting Information, Figure S13) and represents the (2−4) dimer, which is still stable at room temperature (Figure 10, panel B). The absence of the 1723 cm^{-1} band at 383 K (Supporting Information, Figure S14) is also in agreement with the theoretical results that the (2−4) dimer is no longer stable at 383 K.

CONCLUSIONS

The dynamics of hydrogen bonds in a supramolecular system have been studied using a multidisciplinary approach, from synthesis and spectroscopic characterization to computational analysis. Two prototypical uracil derivatives were studied using infrared spectroscopy and complemented by ab initio molecular dynamics calculations. Matrix isolation IR (MI-IR) spectroscopy provided spectra of isolated monomers and isolated dimers. The combination of MI-IR and temperature-dependent IR spectroscopy opens new possibilities in the study of supramolecular hydrogen bonded systems. By following the evolution of vibrational peaks affected by H-bonds with increasing temperature, the weakening and subsequent disruption of hydrogen bonds was identified at temperatures around 330−390 K. Large-scale ab initio molecular dynamics calculations were used to investigate this phenomenon theoretically and pinpointed the processes responsible for H-bond disruption: starting with more or less rigid dimers at room temperature, the melting is gradually induced by large thermal fluctuations in the dimers that lead a thermal equilibrium between different dimer configurations in the potential energy surface at intermediate temperatures. Above the sublimation temperatures for the two molecules, the H-bonds are finally disrupted, illustrating that the sublimation temperature provides a good estimate for H-bond stability in such systems.

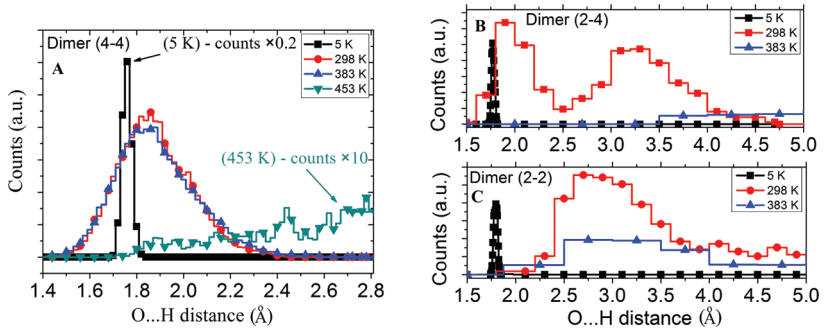

Figure 10. Histogram of the evolution of the O···H distance at different temperatures as obtained from the AIMD calculations; (A) (4−4) dimer, (B) (2−4) dimer, and (C) (2−2) dimer. Some data were scaled as indicated in the figure.

dx.doi.org/10.1021/jp212115h | J. Phys. Chem. B 2012, 116, 4626−4633

The melting of H-bonds was studied in both uracil derivative molecules. Experimental and theoretical investigations reveal the mechanism behind H-bond breaking. H-bonding patterns are completely locked in at cryogenic temperatures. Around room temperature, the amplitude of the H-bond affected vibrations increases significantly, and we get dynamic conformer exchange, which leads to broadening of the H-bonded peaks. Further temperature increase above the sublimation temperature of each molecule (determined during the matrix isolation experiment) leads to melting of the system. On the basis of the calculated O···H distances as a function of temperature, the H-bond disruption temperature region was found to be in accordance with experimental data. We consider this a very important result: reliable predictions from molecular dynamics calculations can greatly reduce the cost and effort of determining hydrogen bond dynamics in systems important for biology or nanoscience.

■ ASSOCIATED CONTENT

Supporting Information

Details of synthetic procedures, additional IR spectra, details of the MD-IR peak assignment, and movies following the trajectory of AIMD simulations at different temperatures. This material is available free of charge via the Internet at http://pubs.acs.org.

■ AUTHOR INFORMATION

Corresponding Author

*E-mail: szekrenyes.zsolt@wigner.mta.hu.

Notes

The authors declare no competing financial interest.

■ ACKNOWLEDGMENTS

This research was supported by the European Union through the Marie Curie Research Training Network PRAIRIES, contract MRTN-CT-2006-035810. Allocations of computer resources at the University of Liverpool, the Science and Technology Facilities Council, and by the SNAC are also gratefully acknowledged. The MI work was funded by the Hungarian Scientific Research Fund (grant no. OTKA K75877); the European Union and the European Social Fund have provided financial support to the project under the grant agreement no. TÁMOP 4.2.1./B-09/KMR-2010-0003.

■ REFERENCES

(1) Ciesielski, A.; Palma, C.-A.; Bonini, M.; Samorì, P. *Adv. Mater.* **2010**, *22*, 3506.
(2) Rossi, M.; Blum, V.; Kupser, P.; von Helden, G.; Bierau, F.; Pagel, K.; Meijer, G.; Scheffler, M. *J. Phys. Chem. Lett.* **2010**, *1*, 3465−3470.
(3) Tkatchenko, A.; Rossi, M.; Blum, V.; Ireta, J.; Scheffler, M. *Phys. Rev. Lett.* **2011**, *106*, 118102.
(4) Blunt, M. O.; Russell, J. C.; del Carmen Giminez-Lopez, M.; Garrhan, J. P.; Lin, X.; Schröder, M.; Champess, N. R.; Beton, P. H. *Science* **2008**, *322*, 1077.
(5) Palma, C.-A.; Bjork, J.; Bonini, M.; Dyer, M. S.; Llanes-Pallas, A.; Bonifazi, D.; Persson, M.; Samorì, P. *J. Am. Chem. Soc.* **2009**, *131*, 13062−13071.
(6) Ciesielski, A.; Stefankiewicz, A. R.; Hanke, F.; Persson, M.; Lehn, J. M.; Samorì, P. *Small* **2011**, *7*, 342.
(7) Blight, B. A.; Hunter, C. A.; Leigh, D. A.; McNab, H.; Thomson, P. I. T. *Nat. Chem.* **2011**, *3*, 246−250.
(8) Jeffrey, G. A.; Saenger, W. *Hydrogen Bonding in Biological Structures*; Springer-Verlag: Berlin, Germany, 1991.
(9) Piot, L.; Palma, C.-A.; Llanes-Pallas, A.; Prato, M.; Szekrényes, Z.; Kamarás, K.; Bonifazi, D.; Samorì, P. *Adv. Funct. Mater.* **2009**, *19*, 1207.
(10) Barth, J. V.; Costantini, G.; Kern, K. *Nature* **2005**, *437*, 671.
(11) Surin, M.; Samorì, P. *Small* **2007**, *3*, 190.
(12) Llanes-Pallas, A.; Matena, M.; Jung, T.; Prato, M.; Stöhr, M.; Bonifazi, D. *Angew. Chem., Int. Ed.* **2008**, *47*, 7726.
(13) Palma, C.-A.; Bonini, M.; Llanes-Pallas, A.; Breiner, T.; Prato, M.; Bonifazi, D.; Samorì, P. *Chem. Commun.* **2008**, *2008*, 5245.
(14) Llanes-Pallas, A.; Palma, C.-A.; Piot, L.; Belbakra, A.; Listorti, A.; Prato, M.; Samorì, P.; Armaroli, N.; Bonifazi, D. *J. Am. Chem. Soc.* **2009**, *131*, 509.
(15) Bonifazi, D.; Mohnani, S.; Llanes-Pallas, A. *Chem.—Eur. J.* **2009**, *15*, 7004−7015.
(16) Mohnani, S.; Llanes-Pallas, A.; Bonifazi, D. *Pure Appl. Chem.* **2010**, *82*, 917−929.
(17) Hadzi, D.; Bratos, S. *Vibrational Spectroscopy of the Hydrogen Bond*; North-Holland: Amsterdam, The Netherlands, 1976.
(18) Griffiths, P. R.; de Haseth, J. A. *Fourier Transform Infrared Spectrometry*, 2nd ed.; John Wiley & Sons, Inc.: Hoboken, N.J., 2007.
(19) Kavitha, V.; Sankaran, K.; Viswanathan, K. S. *J. Mol. Struct.* **2006**, *791*, 165.
(20) Barnes, A. J. *J. Mol. Struct.* **1984**, *113*, 161−174.
(21) Dunkin, I. R. *Matrix-Isolation Techniques: A Practical Approach*; Oxford University Press: New York, 1998.
(22) Parry, G. S. *Acta Crystallogr.* **1954**, *7*, 313−320.
(23) Stewart, R. F.; Jensen, L. H. *Acta Crystallogr.* **1967**, *23*, 1102−1105.
(24) Pohl, G.; Perczel, A.; Vass, E.; Magyarfalvi, G.; Tarczay, G. *Phys. Chem. Chem. Phys.* **2007**, *9*, 4698.
(25) Góbi, S.; Knapp, K.; Vass, E.; Majer, Z.; Magyarfalvi, G.; Hollósi, M.; Tarczay, G. *Phys. Chem. Chem. Phys.* **2010**, *12*, 13603.
(26) Blum, V.; Gehrke, R.; Hanke, F.; Havu, P.; Havu, V.; Ren, X.; Reuter, K.; Scheffler, M. *Comput. Phys. Commun.* **2009**, *180*, 2175.
(27) Perdew, J. P.; Burke, K.; Ernzerhof, M. *Phys. Rev. Lett.* **1996**, *77*, 3865−3868.
(28) Tkatchenko, A.; Scheffler, M. *Phys. Rev. Lett.* **2009**, *102*, 073005.
(29) Jurečka, P.; Šponer, J.; Černỳ, J.; Hobza, P. *Phys. Chem. Chem. Phys.* **2006**, *8*, 1985−1993.
(30) Hanke, F. *J. Comput. Chem.* **2011**, *32*, 1424.
(31) Bussi, G.; Donadio, D.; Parrinello, M. *J. Chem. Phys.* **2007**, *126*, 014101.
(32) Biemann, L.; Häber, T.; Kleinermanns, K. *J. Chem. Phys.* **2009**, *130*, 125102.
(33) Ramírez, R.; López-Ciudad, T.; Kumar, P.; Marx, D. *J. Chem. Phys.* **2004**, *121*, 3973.
(34) Egorov, S. A.; Skinner, J. L. *Chem. Phys. Lett.* **1998**, *293*, 469.
(35) Bahn, S.; Jacobsen, K. *Comput. Sci. Eng.* **2002**, *4*, 56.
(36) Feyer, V.; Plekan, O.; Richter, R.; Correno, M.; Vall-llosera, G.; Prince, K. C.; Trofimov, A. B.; Zaytseva, I. L.; Moskovskaya, T. E.; Gromov, E. V.; Schirmer, J. *J. Phys. Chem. A* **2009**, *113*, 5736−5742.
(37) Choi, M. Y.; Miller, R. E. *J. Phys. Chem. A* **2007**, *111*, 2475−2479.
(38) Tian, S.; Zhang, C.; Zhang, Z.; Chen, X.; Xu, K. *Chem. Phys.* **1999**, *242*, 217−225.
(39) López, C.; Claramunt, R. M.; Alkorta, I.; Elguero, J. *Spectroscopy* **2000**, *14*, 121−126.
(40) Les, A.; Adamowicz, L. *J. Phys. Chem.* **1989**, *93*, 7078.
(41) Leszczynski, J. *J. Phys. Chem.* **1992**, *96*, 1649.
(42) Estrin, D. A.; Paglieri, L.; Corongiu, G. *J. Phys. Chem.* **1994**, *98*, 5653.